Check for updates

ChemPhysChem

Chemistry Europe
European Chemical Societies Publishing

Accepted Article

Title: Photodetachment Dynamics and Structural Flexibility of Undercoordinated Iridium Halides $IrCl_n^-$ (n = 3−5): An Experimental and Theoretical Investigation

Authors: Peng Tang, Jian Zhang, Xueying Li, Fan Yang, Zhubin Hu, Haitao Sun, Xue-Bin Wang, Zhenrong Sun, and Yan Yang

This manuscript has been accepted after peer review and appears as an Accepted Article online prior to editing, proofing, and formal publication of the final Version of Record (VoR). The VoR will be published online in Early View as soon as possible and may be different to this Accepted Article as a result of editing. Readers should obtain the VoR from the journal website shown below when it is published to ensure accuracy of information. The authors are responsible for the content of this Accepted Article.

To be cited as: *ChemPhysChem* **2025**, e202500170

Link to VoR: https://doi.org/10.1002/cphc.202500170

WILEY VCH

14397641, ja, Downloaded from https://chemistry-europe.onlinelibrary.wiley.com/doi/10.1002/cphc.202500170 by Battelle Memorial Institute, Wiley Online Library on [26/05/2025]. See the Terms and Conditions (https://onlinelibrary.wiley.com/terms-and-conditions) on Wiley Online Library for rules of use; OA articles are governed by the applicable Creative Commons License

Accepted Manuscript

Photodetachment Dynamics and Structural Flexibility of Undercoordinated Iridium Halides $IrCl_n^-$ (n = 3–5): An Experimental and Theoretical Investigation

Peng Tang[+],[a] Jian Zhang[+],[b] Xueying Li,[a] Fan Yang,[a] Zhubin Hu,[a] Haitao Sun,[a] Xue-Bin Wang,[c] Zhenrong Sun,[*][a][d] and Yan Yang[*][a]

[a] State Key Laboratory of Precision Spectroscopy, East China Normal University, Shanghai 200241, China.

[b] College of Chemistry & Chemical Engineering, Donghua University, Shanghai 201620, China

[c] Physical Sciences Division, Pacific Northwest National Laboratory, Richland, WA 99352, USA.

[d] Collaborative Innovation Center of Extreme Optics, Shanxi University, Taiyuan, Shanxi 030006, China

[*] Corresponding author at: State Key Laboratory of Precision Spectroscopy, School of Physics and Electronic Science, East China Normal University, Shanghai 200241, P. R. China. E-mail address: yyang@lps.ecnu.edu.cn (Y. Yang). State Key Laboratory of Precision Spectroscopy, School of Physics and Electronic Science, East China Normal University, Shanghai 200241, P. R. China. E-mail address: zrsun@phy.ecnu.edu.cn (Z. R. Sun)

[+] These authors contributed equally to this paper.

Abstract: Three undercoordinated iridium chloride anions, $IrCl_n^-$ (n = 3–5), and their neutral counterparts were investigated by cryogenic anion photoelectron spectroscopy and theoretical calculations. Photodetachment of $IrCl_n^-$ leads to formation of the corresponding neutral complex, *i.e.*, a triplet ground state for n = 3, a quartet for n = 4, and close-lying singlet and triplet for n = 5. The vertical detachment energies are determined to be 3.89, 4.98, and 5.14 eV for n = 3, 4, and 5, respectively, revealing superhalogen anion properties with increasing electron detachment energies as chloride ligands added. The $IrCl_3^-$ spectrum features an extremely broad, lowest electron binding energy band, attributed to resonant autodetachment with prominent non-Franck–Condon profiles. In $IrCl_5^-$, detachment prompts a *d*-orbital rearrangement that drives a structural transformation from a twisted square-based pyramidal (SBP) to a trigonal-bipyramidal (TBP) geometry in the singlet state. These findings provide insights into

This article is protected by copyright. All rights reserved.

the electronic and structural adaptability of iridium halides, advancing our understanding of ligand exchange reactions and dissociative stability in transition metal complexes.

Introduction

Iridium is renowned as the most corrosion-resistant metal and one of the rarest elements, making it highly valuable across various fields.[1] Its exceptional ability to form stable bonds with diverse molecules and ions has enabled the development of versatile iridium complexes with extensive applications in cancer therapy,[2-6], cell imaging,[7-10] catalytic oxidation,[11-15]electroluminescent devices,[16-19] and beyond.[20-22]

Given the broad utility of iridium complexes, substantial experimental and theoretical studies have been performed on iridium halides as archetypal coordination complexes. These studies aim to elucidate their physicochemical properties, including geometries, electron affinities, electronic configuration, bonding characteristics, and more.[23-32] For instances, in 1978, Clark et al. investigated the absorption spectra of $IrCl_6^{2-}$ and $IrBr_6^{2-}$ in solution using resonance Raman spectroscopy.[23] Wang and Wang employed negative ion photoelectron spectroscopy (NIPES) to study the isolated hexahalogenometallate dianions $[ML_6]^{2-}$ (M=Re, Os, Ir, Pt; L=Cl and Br) generated via electrospray ionization (ESI), providing rich electronic structure information for these classical transition-metal halide complexes with direct estimates of their repulsive Coulomb barriers (RCBs) along the electron detachment coordinates[25]. Marcum et al. examined the photodissociation behavior of $IrBr_6^{2-}$ in both solution and the gas phases, observing distinct solvatochromic shifts under visible and ultraviolet light irradiation.[26] Despite these advances, most research has focused on coordinatively saturated iridium halides and their photodissociation mechanisms, leaving undercoordinated iridium halides largely unexplored. These undercoordinated species, however, emerge as crucial intermediates in iridium related cancer therapeutics and catalysis. Therefore, it is highly desirable to study their geometries, electronic structures, and photochemical reactions to shed light on the fundamental chemical transformations and underlying therapeutic mechanisms.

Over the years, NIPES has become a powerful spectroscopic means for studying geometrical and electronic structures of anions, exploring quantum chemical reaction dynamics, and probing noncovalent host-guest interaction strengths.[33-37] Herein, we report a combined experimental and theoretical investigation of three-, four-, and five-coordinated iridium chloride anions $IrCl_n^-$ (n = 3–5) using a custom-built cryogenic anion cluster photoelectron spectroscopy (CRACPES) apparatus.[37] By optimizing the voltage parameters of a dual ion funnel system, we efficiently generated adequate amounts of target anions that would be otherwise challenging to produce. The vertical (VDE) and adiabatic detachment energies (ADE) of $IrCl_n^-$, derived from the photoelectron spectra, increase with the number of chloride ions, and are well

This article is protected by copyright. All rights reserved.

14397641, ja, Downloaded from https://chemistry-europe.onlinelibrary.wiley.com/doi/10.1002/cphc.202500170 by Battelle Memorial Institute, Wiley Online Library on [26/05/2025]. See the Terms and Conditions (https://onlinelibrary.wiley.com/terms-and-conditions) on Wiley Online Library for rules of use; OA articles are governed by the applicable Creative Commons License

Accepted Manuscript

14397641, ja, Downloaded from https://chemistry-europe.onlinelibrary.wiley.com/doi/10.1002/cphc.202500170 by Battelle Memorial Institute, Wiley Online Library on [26/05/2025]. See the Terms and Conditions (https://onlinelibrary.wiley.com/terms-and-conditions) on Wiley Online Library for rules of use; OA articles are governed by the applicable Creative Commons License

Accepted Manuscript

reproduced by density functional theory (DFT) calculations. Upon interaction with a laser field, $IrCl_n^-$ (n = 3–5) anions can undergo two distinct excitation processes depending on the photon energy: direct photodetachment and resonant excitation. In the direct photodetachment pathway, photon absorption results in the prompt ejection of an electron from the anion, leading to the formation of a neutral species. This process typically occurs within the Franck–Condon region and accounts for the majority of the signals observed in conventional photoelectron spectroscopy.[38-42] Alternatively, when the photon energy matches a resonant electronic transition of the anion, excitation to an electronically excited anionic state can take place. Such excited states are often metastable and can relax via two competing mechanisms: autodetachment, wherein the excited anion spontaneously emits an electron and transitions to a neutral ground state, and photodissociation, wherein the excited anion dissociates into smaller fragments. In certain cases, fragment anions produced by photodissociation may subsequently absorb additional photons and undergo further direct photodetachment.[25, 43] Therefore, the characteristics of Cl anion was observed in the spectra of $IrCl_4^-$ and $IrCl_5^-$. Franck-Condon simulations and molecular orbital analyses reveal resonant autodetachment in $IrCl_3^-$, and detachment-induced rearrangement of the *d*-orbitals in $IrCl_5^-$ that leads to a singlet ground state with an extremely close-lying triplet for the corresponding neutral.

Experimental and Computational Methodologies

CRACPES Experiments

The detail of the CRACPES setup was reported in a previous publication,[44] and only the essential experimental parameters relevant to the current study are given here. Briefly, a 2 mM dry acetonitrile solution of $(NH_4)_2IrCl_6$ (Shanghai Yuanye Bio-Technology) was prepared and sprayed with a 2 μL/min pump rate and −2.25 kV voltage. After desolvation in a heated capillary, the target anions $IrCl_n^-$ (n = 3−5) were generated via collision-induced dissociation (CID) of the parent $[IrCl_6]^{2-}$ dianions in a two-stage ion funnel by carefully tuning the corresponding DC gradients and RF peak-to-peak voltages, subsequently guided and mass-selected using two quadrupole mass filters. These fragment "hot" anions were then cooled and enriched in a cryogenic two-stage linear ion trap (set at 13 Kevin) downstream through collisions with cold helium buffer gas. The cryogenically cooled anions were extracted out from the trap, mass-selected in a time-of-flight (TOF) mass spectrometer, underwent momentum deceleration to minimize Doppler broadening, and interrogated with 193 nm photons in the interaction zone. The resulting photoelectrons were collected and analyzed using a magnetic-bottle type photoelectron spectrometer. The laser was running at 50 Hz while the anions were pulsed out at 25 Hz to afford shot-to-shot background subtraction. The TOF photoelectron spectrum was calibrated using the known I^- [45] and MnO_4^- [46] spectra with an energy resolution (ΔE/E) of 1.9 % (i.e., 30 meV full width at half maximum for the electrons with kinetic energy of 1.60 eV). The experimental VDE was

This article is protected by copyright. All rights reserved.

14397641, ja, Downloaded from https://chemistry-europe.onlinelibrary.wiley.com/doi/10.1002/cphc.202500170 by Battelle Memorial Institute, Wiley Online Library on [26/05/2025]. See the Terms and Conditions (https://onlinelibrary.wiley.com/terms-and-conditions) on Wiley Online Library for rules of use; OA articles are governed by the applicable Creative Commons License

Accepted Manuscript

determined from the peak maximum of the first band (lowest electron binding energy (eBE)) in the spectrum, while the ADE was estimated by drawing a straight line along the rising edge of the first band and adding the instrumental resolution to the intersection point with the eBE axis.

Computational Methods

The initial geometries of $IrCl_n^-$ (n = 3−5) anions and corresponding neutrals were constructed according to the general molecular orbital theory of transition metal (TM) complexes.[47] These structures under different spin multiplicities were fully optimized by density functional theory (DFT) using the hybrid B3LYP-D3(BJ) exchange-correlation functional[48, 49] that has been widely employed for 5d TM complexes.[27-30, 50-53] The aug-cc-pVTZ basis set was used for Cl atoms,[54] while the effective core potential (ECP) basis set aug-cc-pVTZ-pp was adopted for Ir atom,[55] to account for the scalar relativistic effects.[55-58] Harmonic vibrational frequencies were calculated to confirm the absence of imaginary frequencies in the optimized geometries. Single-point energy calculations for $IrCl_n^-$ anions and neutrals were subsequently computed by coupled cluster calculations with single, double, and perturbative triple excitations (CCSD(T))[59] using the same basis sets. The ADE was calculated as the energy difference between the neutral and anion at their respective optimized geometries with zero-point-energy (ZPE) corrections, while the VDE was calculated as the energy difference of the neutral and anion both at the optimized anion structure. Additionally, natural bond orbital (NBO) charge distributions, charge density differences (CDD), spin natural orbitals (SNO), and molecular orbital (MO) analyses were conducted at the B3LYP-D3(BJ)//aug-cc-pVTZ-(pp) level for each anion and corresponding neutral. However, spin-orbit coupling was not included in the calculations, which might affect the accuracy of the computed excited-state energies.[60-62] All calculations were conducted using the GAUSSIAN16 software packages,[63] while Multiwfn[64] and VMD tools[65] were employed for NBO, CDD, SNO, MO analyses and visualization. Frank-Condon factors (FCFs) were simulated using the ezSpectrum program.[66]

Results and Discussion

Photoelectron Spectra of $IrCl_n^-$ (n = 3−5)

The NIPE spectra of $IrCl_n^-$ (n=3−5) irradiated by a 193 nm laser with the trap temperature set at 13 K are shown in Figure 1. Six spectral bands are observed in the eBE range of 3.5-6.4 eV for n = 3 (labelled as X, A-E in the ascending eBE order), while six peaks are seen between 4.8 and 6.4 eV for n = 4, and only four bands are resolved starting from eBE = 5.1eV for n = 5. Additionally, a peak at eBE = 3.62 eV is clearly seen in each of the n = 4 and 5 spectrum, corresponding to photodetachment of Cl^-, a photodissociation product of $IrCl_4^-$ and $IrCl_5^-$, reported by Wang and Marcum et

This article is protected by copyright. All rights reserved.

al as well.[25, 28] Close inspection of the rising edge of the X band in $IrCl_3^-$ reveals a shoulder at eBE ~ 3.6 eV, indicating that this photodissociation-photodetachment Cl^- may also occur to certain degree. The rising slope of the X band in the n = 3 spectrum is appreciably smaller compared to those for n = 4 and 5. The experimental VDEs are measured from the maximum of each X band to be 3.89, 4.98, and 5.14 eV, while the corresponding ADEs, estimated from the X band threshold are 3.57, 4.76, and 4.99 eV, for n = 3−5, respectively (Table 2). The eBE of $IrCl_n^-$ increases with the number of Cl^-, and clearly exceeds the electron affinity of the Cl atom beyond n = 3. We performed density-of-states (DOS) simulations based on Koopmans' approximation for $IrCl_3^-$, $IrCl_4^-$, and $IrCl_5^-$. As shown in the Figure 1, the blue stick spectra represent the simulated DOS of neutral states accessible via photodetachment. These simulations qualitatively reproduce the overall envelope of the experimental spectra (red curves), particularly in the regions beyond the vibrationally structured X bands.

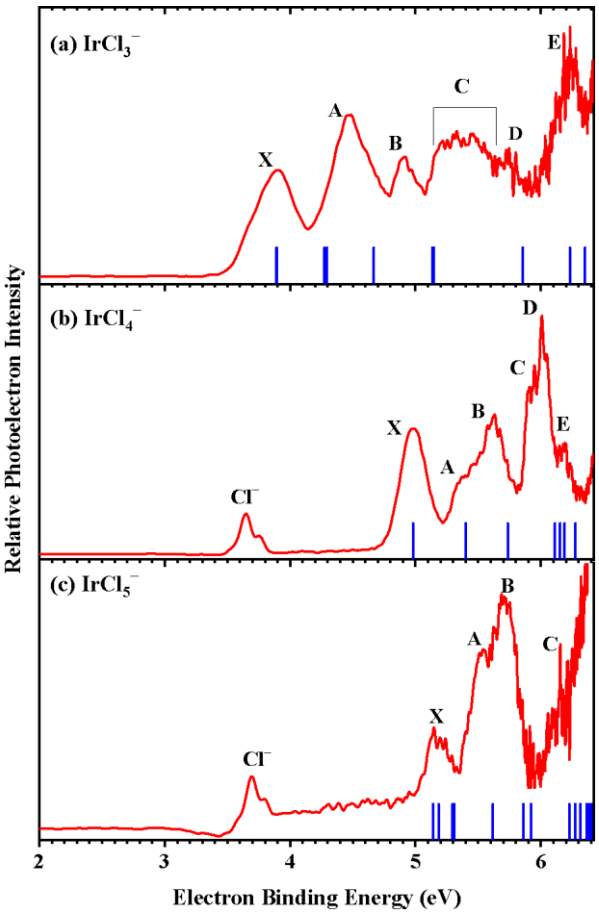

Figure 1. Cryogenic photoelectron spectra of $IrCl_3^-$ (a), $IrCl_4^-$ (b), and $IrCl_5^-$ (c) recorded with 193 nm photons and at 13 K temperature. Density of states (blue sticks) of each anion were simulated at the B3LYP(BJ)/aug-cc-pVTZ-(pp) level.

Geometrical Structures of $IrCl_n^{-/0}$ (n = 3−5)

Table 1 summarizes the B3LYP-D3(BJ)/aug-cc-pVTZ-(pp) optimized lowest-energy geometries of the $IrCl_n^-$ anions and neutrals with their spin multiplicities, bond lengths (in Å) and bond angles (in degrees) listed. Identical numbering is used for the

This article is protected by copyright. All rights reserved.

14397641, ja, Downloaded from https://chemistry-europe.onlinelibrary.wiley.com/doi/10.1002/cphc.202500170 by Battelle Memorial Institute, Wiley Online Library on [26/05/2025]. See the Terms and Conditions (https://onlinelibrary.wiley.com/terms-and-conditions) on Wiley Online Library for rules of use; OA articles are governed by the applicable Creative Commons License

Accepted Manuscript

10.1002/cphc.202500170

1 Cl ligands with equivalent Ir-Cl bond lengths and roles within the molecular structure.

2 **Table 1.** B3LYP−D3(BJ)/aug−cc−pVTZ−(pp) optimized structures of the lowest energy anions
3 $IrCl_n^-$ (n = 3−5) and their corresponding neutrals.

Anions/Neutrals	**$IrCl_3^-$**	**$IrCl_3$**	**$IrCl_4^-$**	**$IrCl_4$**
Spin Multiplicity	doublet	Triplet[#]	triplet	Quartet[#]
Optimized geometries	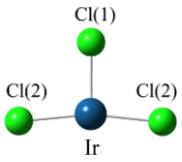	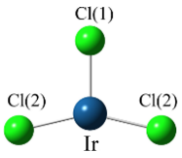	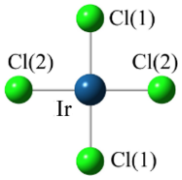	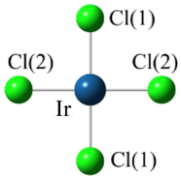
Ir−Cl(1)	2.273	2.205	2.299	2.244
Ir−Cl(2)	2.291	2.201	2.299	2.244
∠Cl(1)−Ir−Cl(2)	95.8	103.2	90.0	90.0
∠Cl(2)−Ir−Cl(2)	168.4	153.5	180.0	180.0

Anions/Neutrals	**$IrCl_5^-$**	**$IrCl_5$**	**$IrCl_5$**
Spin Multiplicity	doublet	singlet	triplet
Optimized geometries	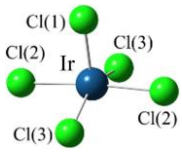	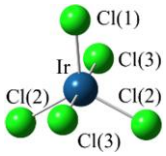	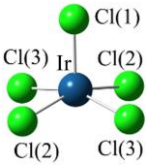
Ir−Cl(1)	2.223	2.183	2.189
Ir−Cl(2)	2.371	2.183	2.280
Ir−Cl(3)	2.284	2.351	2.280
∠Cl(1)− Ir−Cl(2)	92.6	120.0	101.0
∠Cl(2)− Ir−Cl(2)	174.9	120.0	158.0
∠Cl(1)− Ir−Cl(3)	104.4	90.0	101.0
∠Cl(2)− Ir−Cl(3)	89.4	90.0	87.9
∠Cl(3)− Ir−Cl(3)	151.2	180.0	158.0

This article is protected by copyright. All rights reserved.

14397641, ja, Downloaded from https://chemistry-europe.onlinelibrary.wiley.com/doi/10.1002/cphc.202500170 by Battelle Memorial Institute, Wiley Online Library on [26/05/2025]. See the Terms and Conditions (https://onlinelibrary.wiley.com/terms-and-conditions) on Wiley Online Library for rules of use; OA articles are governed by the applicable Creative Commons License

Accepted Manuscript

14397641, ja, Downloaded from https://chemistry-europe.onlinelibrary.wiley.com/doi/10.1002/cphc.202500170 by Battelle Memorial Institute, Wiley Online Library on [26/05/2025]. See the Terms and Conditions (https://onlinelibrary.wiley.com/terms-and-conditions) on Wiley Online Library for rules of use; OA articles are governed by the applicable Creative Commons License

Accepted Manuscript

The corresponding lowest energy singlet for the n=3 and doublet for the n = 4 are predicted to be triangular pyramid and saddle shape which are less stable by 0.23 and 0.28 eV, respectively.

The ground state of $IrCl_3^-$ adopts a T-shaped planar structure with a doublet spin multiplicity. The Ir-Cl bond lengths are 2.273 Å for the apical bond and 2.291 Å for the basal bond. Upon electron detachment, the most stable neutral $IrCl_3$ assumes a Y-shaped structure with a triplet spin multiplicity, where the apical and basal Ir-Cl bond lengths contract to 2.205 and 2.201 Å, respectively. Its singlet analog is predicted to be a triangular pyramid structure, less stable by 0.23 eV (Figure S1).

For $IrCl_4^-$, the lowest-energy structure has a triplet square planar geometry, with the Ir atom centrally positioned within a square formed by four equivalent Cl ligands, each with an Ir-Cl bond length of 2.299 Å. Following electron detachment, the ground state of the neutral $IrCl_4$ retains a square planar geometry with a quartet spin multiplicity, and the bond lengths decrease to 2.244 Å. The doublet $IrCl_4$ is calculated to have a saddle shape and lie 0.28 eV higher in energy (Figure S1).

$IrCl_5^-$ adopts a twisted square-based pyramidal (SBP) geometry with a doublet spin multiplicity, where the four Cl ligands forming the base are non-coplanar, and the Ir-Cl bonds along the diagonal are equivalent. Upon electron detachment, two close-lying isomers are found for the neutral $IrCl_5$ with the lowest energy structure being singlet and 30 meV (0.69 kcal/mol) more stable than its triplet counterpart (Figure S1).

The singlet $IrCl_5$ adopts a trigonal-bipyramidal (TBP) structure, characterized by three equatorial Cl ligands with bond angles of 120° and two axial Cl ligands perpendicular to the equatorial plane. In contrast, the triplet $IrCl_5$, which is 30 meV higher in energy than the singlet $IrCl_5$, retains an SBP geometry with the Ir atom displaced above the square base and the apex/base Ir-Cl bond length of 2.189/2.280 Å. Interestingly, among the two neutral $IrCl_5$ isomers, the triplet state, despite having slightly higher energy, more closely mirrors the structural characteristics of the doublet $IrCl_5^-$ anion, both in bond lengths and bond angles, compared to the singlet TBP neutral state.

Calculated VDEs and ADEs of $IrCl_n^-$ (n = 3−5)

Table 2. Experimental and theoretical ADEs and VDEs calculated at the CCSD(T)/aug-cc-pVTZ(-pp) level of theory.

Value / Anion [a]	VDE (eV)		ADE (eV)	
	Calc.	Exp.	Calc.	Exp.
$IrCl_3^-$ (to singlet)	4.80	3.89 ± 0.05	3.61	3.57 ± 0.05 [b]
$IrCl_3^-$ (to triplet)	3.77		3.38	
$IrCl_4^-$ (to doublet)	5.87	4.98 ± 0.05	4.74	4.76 ± 0.05
$IrCl_4^-$ (to quartet)	4.65		4.46	

This article is protected by copyright. All rights reserved.

14397641, ja, Downloaded from https://chemistry-europe.onlinelibrary.wiley.com/doi/10.1002/cphc.202500170 by Battelle Memorial Institute, Wiley Online Library on [26/05/2025]. See the Terms and Conditions (https://onlinelibrary.wiley.com/terms-and-conditions) on Wiley Online Library for rules of use; OA articles are governed by the applicable Creative Commons License

Accepted Manuscript

$IrCl_5^-$ (to singlet)	5.36	5.14 ± 0.05	4.90	4.99 ± 0.05
$IrCl_5^-$ (to triplet)	5.16		4.93	

[a] The anion transitions shown in bold fond are those that contribute to the experimental X bands.
[b] The number only represents an experimental apparent ADE since the onset threshold signal of $IrCl_3^-$ is significantly influenced by a resonant autodetachment process (see the discussion below of Fig.3).

Based on the above optimized lowest-energy structures, the CCSD(T)/aug-cc-pVTZ(-pp) ADEs and VDEs were calculated and compared with the experimental values in Table 2. For $IrCl_3^-$ and $IrCl_4^-$, the calculated values are slightly smaller than the experimental measurements by 0.1-0.2 for the former and 0.3 eV for the latter. For $IrCl_5^-$, because there exist two close-lying, yet distinct transitions corresponding to the singlet and triplet neutral state that could contribute to the experimental X band, we computed two sets of ADE and VDE. The calculated ADEs for both excitations align closely with the experimental value. However, the VDE calculations indicate a clear better match with the experimental data for the transition to the isomeric triplet $IrCl_5$ that is higher in energy rather than to the most stable singlet state. This abnormality warrants further examination and will be discussed in detail below.

NBO Charge Distribution and CDD Analyses

To help elucidate the relevant photodetachment processes, we conducted NBO charge distribution and charge density difference (CDD) analyses for each anion and its corresponding neutral species. Table 3 provides the NBO charge distributions of $IrCl_n^{-/0}$ along with the component charge contributions of Ir and Cl_n ligands during both vertical and adiabatic detachment processes. For all anions, the excess negative charge is primarily localized on the Cl ligands, from which the photoelectron is predominately detached. The central Ir atom retains a positive charge in $IrCl_n^-$ due to the strong electron-withdrawing nature of the Cl ligands. The central Ir atom also loses noticeable negative charges in the photodetachment of $IrCl_3^-$ and $IrCl_4^-$, while no appreciable charge difference on Ir is found for $IrCl_5^-$. Notably, Ir loses a greater negative charge during the vertical detachment than that in the adiabatic process, suggesting that the geometry relaxation transfers certain electron density from the ligands back to the central metal atom.

Table 3. The B3LYP-D3(BJ)/aug−cc−pVTZ(−pp) calculated NBO charge distributions in $IrCl_n^-$ and $IrCl_n$ (n = 3−5) for both vertical and adiabatic detachment processes.

Anions	**Ir**	**Cl_n (n =3−5)**	**Neutrals**	**Ir(Vert./Adia.)**	**Cl_n (n =3−5) (Vert./Adia.)**
$IrCl_3^-$	0.19	−1.19	$IrCl_3$(triplet)	0.48/0.36	−0.48/−0.36
$IrCl_4^-$	0.22	−1.22	$IrCl_4$(quartet)	0.30/0.21	−0.30/−0.21

This article is protected by copyright. All rights reserved.

10.1002/cphc.202500170

14397641, ja, Downloaded from https://chemistry-europe.onlinelibrary.wiley.com/doi/10.1002/cphc.202500170 by Battelle Memorial Institute, Wiley Online Library on [26/05/2025]. See the Terms and Conditions (https://onlinelibrary.wiley.com/terms-and-conditions) on Wiley Online Library for rules of use; OA articles are governed by the applicable Creative Commons License

Accepted Manuscript

$IrCl_5^-$	0.03	−1.03	$IrCl_5$(singlet)	0/−0.11	0/0.11
			$IrCl_5$(triplet)	0.05/−0.05	−0.05/0.05

The CDD analysis supports the above NBO results, revealing that the detached electron originates predominately from the Cl ligands, as illustrated in the left panel of Figure 2. A reduction in charge density on the Cl ligands is observed across all three anions, while the central Ir atom exhibits regions of both charge accumulation and depletion. These CDD patterns closely resemble the respective calculated HOMO of the $IrCl_n^-$ (n=3,4) and HOMO/HOMO-1 of $IrCl_5^-$ anions (Figure 2 right), indicating that the experimental X band in the PES measurement originates from photodetachment of the HOMO and HOMO-1 electrons in the anions. For a more comprehensive view of the molecular orbital distributions involved, readers are referred to the Supporting Information (Table S1).

FCF Simulation

To better interpret the vibrational structures observed in the experimental spectra, Franck–Condon factor (FCF) simulations were performed for the X states of $IrCl_3^-$ and $IrCl_4^-$, as well as the singlet and triplet states of $IrCl_5^-$. As shown in Figure 3, the simulated stick spectra were grouped based on dominant vibrational mode contributions and broadened using a Gaussian function with a full width at half maximum (FWHM) of 30 meV. The red curves represent the experimental spectra, the blue curves are broadened fits of the total stick spectra, and sticks with different colors correspond to different vibrational progressions. The detailed vibrational assignments are provided in Tables S2–S4 and the vibrational modes involved in each transition are visualized in Figure S4.

For the $IrCl_3^-$ X state, the FCF simulation reveals four types of vibrational transitions: $0(0) \rightarrow 1(i\nu_3,1\nu_4)$, $0(0) \rightarrow 1(j\nu_3,2\nu_4)$, $0(0) \rightarrow 1(k\nu_3,3\nu_4)$, and $0(0) \rightarrow 1(m\nu_3,1\nu_6)$. The dominant modes include ν_3 (a Cl–Ir–Cl bending mode), ν_4 (an Ir–Cl asymmetric stretching mode), and ν_6 (an Ir–Cl symmetric stretching mode). These features indicate significant vibrational coupling and are consistent with the displacement vectors between the anion and the neutral species.

For $IrCl_4^-$, two main vibrational transitions contribute to the X band: $0(0) \rightarrow 1(i\nu_1)$ and $0(0) \rightarrow 1(j\nu_9)$. Here, ν_9 corresponds to a symmetric stretching of Ir–Cl bonds, while ν_1 involves asymmetric bending of two Cl–Ir–Cl units. Although the neutral $IrCl_4$ molecule retains a nearly planar geometry upon detachment, all Ir–Cl bonds are shortened, which aligns well with the nature of ν_9 and explains its dominant contribution.

The singlet state of $IrCl_5^-$ exhibits transitions dominated by ν_1 and ν_6 modes, namely $0(0) \rightarrow 1(i\nu_1)$ and $0(0) \rightarrow 1(j\nu_1,1\nu_6)$. Both are associated with coupled and complex bending motions.

This article is protected by copyright. All rights reserved.

14397641, ja, Downloaded from https://chemistry-europe.onlinelibrary.wiley.com/doi/10.1002/cphc.202500170 by Battelle Memorial Institute, Wiley Online Library on [26/05/2025]. See the Terms and Conditions (https://onlinelibrary.wiley.com/terms-and-conditions) on Wiley Online Library for rules of use; OA articles are governed by the applicable Creative Commons License

Accepted Manuscript

For the $IrCl_5^-$ triplet state, multiple coupled modes contribute to the vibrational progression. These include ν_1 (non-symmetric Cl–Ir–Cl bending), ν_4 (symmetric Cl–Ir–Cl bending), and ν_{11} and ν_{12} (Ir–Cl symmetric stretching modes), leading to transitions such as $0(0) \rightarrow 2(i\nu_1)$, $0(0) \rightarrow 2(j\nu_1,1\nu_4)$, $0(0) \rightarrow 2(k\nu_1,1\nu_4,1\nu_{12})$, and $0(0) \rightarrow 2(m\nu_1,1\nu_4,1\nu_{11},1\nu_{12})$. These transitions are clearly distinguishable in the experimental spectrum and correspond well with the computed structural differences between the anionic and neutral species.

Direct detachment and resonant autodetachment of $IrCl_3^-$

The electron affinity (EA) of $IrCl_3$ is estimated by the onset of the first band. However, the broadness of the X band, particularly the pronounced low-binding-energy tail, warrants a detailed analysis to better determine the EA. The photodetachment induces substantial structural changes, including bond length reductions of 0.068 and 0.07 Å, an increase in the ∠Cl(1)−Ir−Cl(2) angle by 7.4°, and a decrease in the ∠Cl(2)−Ir−Cl(2) angle by 14.9°, rendering the true 0–0 vibrational transition largely inaccessible. As shown in Figure 3(a), Franck–Condon factor (FCF) simulations for $IrCl_3^-$ produce a fairly broad, but much narrower spectral profile compared to the experimental X band, indicating these geometric effects alone cannot account for the observed broadening of the X band, particularly the gray-shaded region in Figure 3(a). This discrepancy remains across different temperature assumptions as higher temperatures produce negligible changes in the spectral width (Figure S2). This implies that temperature-induced hot-band excitations are not a significant factor, and rules out hot-band excitation as a plausible explanation. To further assess whether instrumental resolution contributes to the observed broadening, we performed FCF simulations using Gaussian convolution widths of 30 meV (close to instrumental resolution), 50 meV and 75 meV. As shown in Figure 3(a) and Figure S3, regardless of the Gaussian convolution width used, the simulated spectra (blue traces) remain significantly narrower than the experimental X band (red trace), ruling out resolution effects as the primary cause.

In the absence of a tunable laser source, we instead calculated the TDDFT absorption spectrum of $IrCl_3^-$, which exhibits strong transitions near 193 nm, indicating resonant absorption at the experimental photon energy. This suggests that the incident UV photons may promote the anion to an excited electronic state that undergoes nonadiabatic coupling with the neutral state, leading to autodetachment**.** Provisionally, we attribute the broadening to resonant autodetachment processes, supported by a mechanism previously reported for similar spectral anomalies.[67-69] For example, in previous fixed-frequency photodetachment studies on dianionic and fullerene systems, similar broadened low-eBE signals were assigned to resonant autodetachment processes, which typically produce weak or non-FC-like features. In our case, the overlap between the absorption band and the photon energy, combined with significant geometry changes and unmatched spectral envelopes, similarly supports the assignment of the gray-shaded portion of the X band to such a mechanism.

This article is protected by copyright. All rights reserved.

10.1002/cphc.202500170

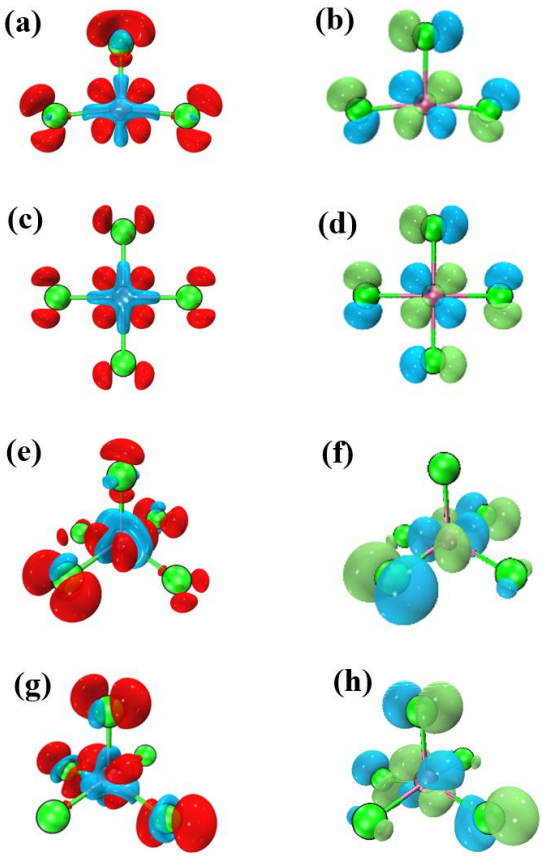

Figure 2. Charge density differences (left panel) in the vertical photodetachment transitions for $IrCl_3^-$ (doublet) → $IrCl_3$ (triplet) (a), $IrCl_4^-$ (triplet) → $IrCl_4$ (quartet) (c), $IrCl_5^-$ (doublet) → $IrCl_5$ (triplet) (e), and $IrCl_5^-$ (doublet) → $IrCl_5$ (singlet) (g) along with their respective HOMOs of $IrCl_3^-$ (b), $IrCl_4^-$ (d), $IrCl_5^-$ (f) and HOMO-1 of $IrCl_5^-$ (h) (right panel, see Table S1 for more frontier molecular orbitals). Color Red (blue) represents the decrease (increase) in charge density with an isovalue of 0.005 au. The Calculations are conducted at the B3LYP-D3(BJ)//aug-cc-pVTZ-(pp) level.

Time-dependent DFT (TDDFT) calculations support this hypothesis, revealing a strong absorption feature near 193 nm (Figure S3(a)), consistent with resonant excitation. This process allows $IrCl_3^-$ to absorb a photon and transition to an excited vibrational manifold of the anion, rather than undergoing direct photodetachment. Large-amplitude nuclear motions in these resonant states enable electron detachment that can be projected across a wide range of vibrational levels in the final neutral $IrCl_3$ surface, including highly excited vibrational states not accessible via direct detachment. Thus, band X contains contributions from direct photodetachment and resonant autodetachment that account for both the low-binding-energy tail and the additional spectral features observed at higher binding energies. A schematic of this process is shown in Figure 4(a).

This article is protected by copyright. All rights reserved.

14397641, ja, Downloaded from https://chemistry-europe.onlinelibrary.wiley.com/doi/10.1002/cphc.202500170 by Battelle Memorial Institute, Wiley Online Library on [26/05/2025]. See the Terms and Conditions (https://onlinelibrary.wiley.com/terms-and-conditions) on Wiley Online Library for rules of use; OA articles are governed by the applicable Creative Commons License

Accepted Manuscript

10.1002/cphc.202500170

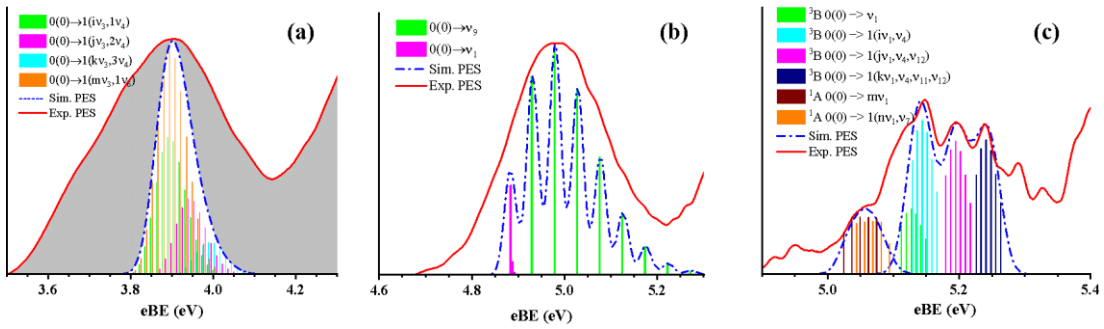

Figure 3. Franck–Condon factor (FCF) simulated spectrum of $IrCl_3^-$ (a), $IrCl_4^-$ (b), and $IrCl_5^-$ (c) superimposed onto the experimental spectrum. The simulated stick positions and intensities of the 0-0 bands have been set to match those in the experimental spectra. Detailed assignments for the involved vibrational excitations are provided in Table S2-S4. The FCF spectra are performed at the (U)B3LYP/6-311+G(2df) level of theory, and the Gaussian broadening is 30 meV.

Unlike $IrCl_3^-$, as shown in Figure 3(b), the simulated FCF profile of $IrCl_4^-$ anions match the experimental spectrum well, and no evidence of resonant autodetachment processes was observed. This is consistent with the anion absorption spectrum (Figure S3(b)) calculated using TDDFT, which shows no absorption peaks near 193 nm.

In the X band of $IrCl_5^-$, as shown in Figure 1(c), a noticeable shoulder is observed in the 5.0 – 5.1 eV eBE range. Since $IrCl_5^-$ does not show resonant absorption at 193 nm (Figure S3(c)), and the temperature-dependent FCF simulations also rule out the possibility of this bump originating from hot band excitation, we attribute this spectral feature to the excitation of $IrCl_5^-$ from its doublet state to the singlet state (^1A) of $IrCl_5$. As discussed earlier, the triplet state (^3B) of the neutral, despite slightly higher in energy than the singlet state, mirrors more closely the structure of the doublet $IrCl_5^-$ anion, compared to the singlet state. Consequently, the Franck–Condon overlap between the doublet ground state of the anion and the triplet state of the neutral species is significantly greater than that with the singlet state (Figure 3(c)), accounting for the observed weak signals in eBE = 5.0-5.1 eV. A schematic excitation diagram is shown in Figure 4(b), in which the VDE to the singlet is 200 meV higher than that to the triplet, although the ADE to the former is 30 meV smaller than the latter (also see Table 2).

This article is protected by copyright. All rights reserved.

14397641, ja, Downloaded from https://chemistry-europe.onlinelibrary.wiley.com/doi/10.1002/cphc.202500170 by Battelle Memorial Institute, Wiley Online Library on [26/05/2025]. See the Terms and Conditions (https://onlinelibrary.wiley.com/terms-and-conditions) on Wiley Online Library for rules of use; OA articles are governed by the applicable Creative Commons License

Accepted Manuscript

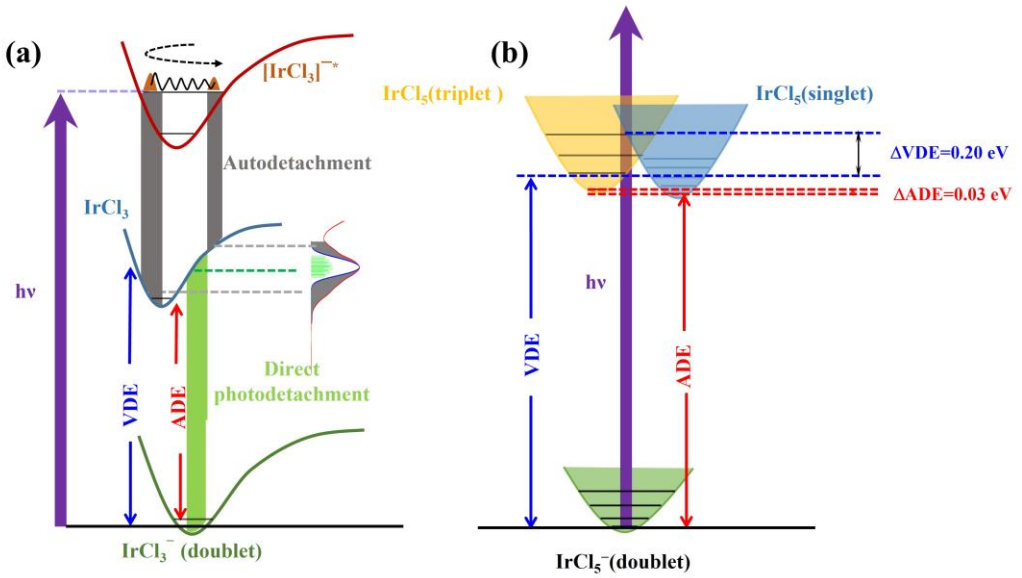

Figure 4. (a) The schematic diagram of autodetachment and direct photodetachment of $IrCl_3^-$. (b) Schematic diagram of photodetachment of $IrCl_5^-$.

The *d*-orbital rearrangement upon detachment leads to structural transformation in $IrCl_5$

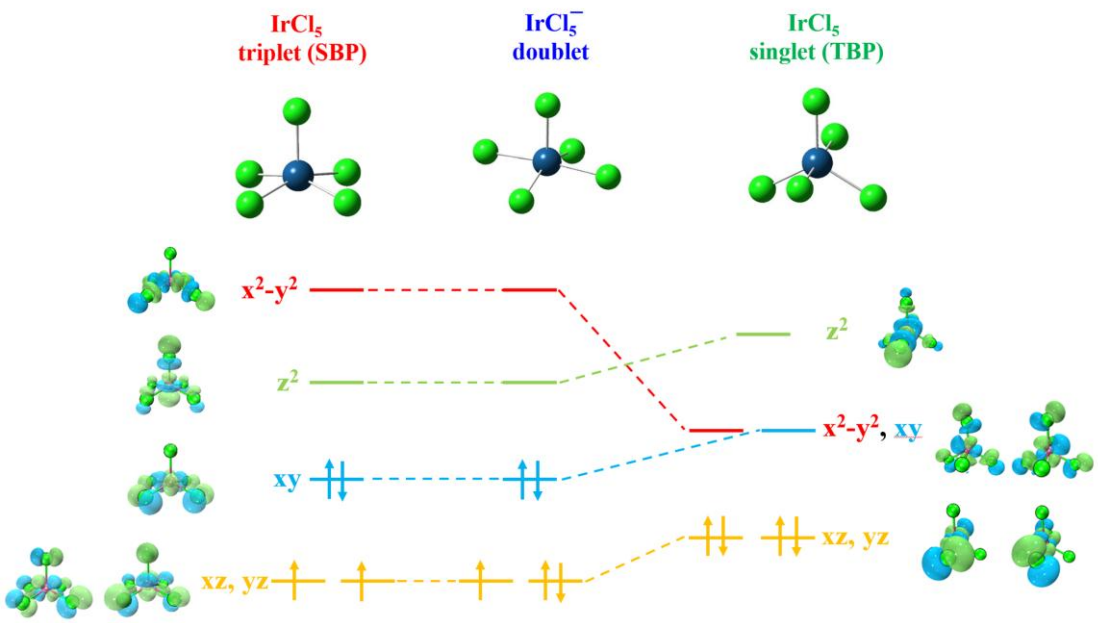

Figure 5. The rearrangement of *d*−orbital after photodetachment.

To further investigate the structural transformation during the detachment of $IrCl_5^-$, the frontier molecular orbitals (FMOs) with significant Ir *d*-orbital contributions are illustrated in Figure . The $IrCl_5^-$ anion can be nominally regarded as derived from an octahedral complex by the removal of one ligand. The five *d*-orbitals are divided into three nonbonding degenerate MOs (d_{xy}, d_{xz}, d_{yz}) and two antibonding degenerate

This article is protected by copyright. All rights reserved.

14397641, ja, Downloaded from https://chemistry-europe.onlinelibrary.wiley.com/doi/10.1002/cphc.202500170 by Battelle Memorial Institute, Wiley Online Library on [26/05/2025]. See the Terms and Conditions (https://onlinelibrary.wiley.com/terms-and-conditions) on Wiley Online Library for rules of use; OA articles are governed by the applicable Creative Commons License

Accepted Manuscript

14397641, ja, Downloaded from https://chemistry-europe.onlinelibrary.wiley.com/doi/10.1002/cphc.202500170 by Battelle Memorial Institute, Wiley Online Library on [26/05/2025]. See the Terms and Conditions (https://onlinelibrary.wiley.com/terms-and-conditions) on Wiley Online Library for rules of use; OA articles are governed by the applicable Creative Commons License

Accepted Manuscript

MOs ($d_{x^2-y^2}$, d_{z^2}) under octahedral coordination. The removal of a ligand along the z-axis reduces an antibonding interaction, stabilizes the d_{z^2} orbital and causes a slight energy splitting between the $d_{x^2-y^2}$ and d_{z^2} orbitals. Structurally, $IrCl_5^-$ adopts a distorted square-based pyramidal (SBP) geometry, with the extra electron disrupting the x-y plane balance and twisting the basal chlorine ligands out of coplanarity with the central Ir.

As shown in Figure 5, Vertical electron detachment from d_{xy} orbital yields neutral triplet $IrCl_5$, and the sequence of *d*-orbital remains the same as $IrCl_5^-$ after relaxation. This results in minimal structural changes and restores the planar arrangement of the basal ligands during the relaxation process, enabling significant Franck–Condon overlap between the doublet $IrCl_5^-$ and triplet $IrCl_5$ during photodetachment.

However, vertical detachment of the electron from the singly occupied d_{xz} orbital produces a closed-shell singlet $IrCl_5$, and the sequence of *d*-orbital changes after relaxation to a trigonal-bipyramidal (TBP) structure. This transition involves substantial *d*-orbital rearrangement, as shown in Figure . In the TBP geometry, the d_{z^2} orbital becomes the highest-energy orbital due to antibonding interactions with all five ligands. Similarly, the d_{xy} and $d_{x^2-y^2}$ orbitals are destabilized by antibonding interactions with the two equatorial ligands, placing them above the weakly bonding d_{xz} /d_{yz} orbitals. This reordering drives the structural transformation from the twisted SBP geometry to the highly symmetric TBP geometry. This orbital and structural rearrangement is energetically favorable for forming the singlet state and explains the distinct spectral features associated with singlet $IrCl_5$. The strong coupling between geometry and electronic structure highlights the critical role of *d*-orbital interactions in determining the detachment pathways and consequential spectral characteristics.

Conclusions

In this study, three undercoordinated iridium halides, $IrCl_n^-$ (n = 3−5), and their neutral counterparts were investigated using cryogenic anion photoelectron spectroscopy and theoretical calculations. These anions exhibit superhalogen characteristic with their VDEs and ADEs increasing as the number of halogen atoms increases. Frontier molecular orbitals (FMOs) and charge density differences analyses indicate that the detachment process predominantly involves the d orbitals of the iridium atom, with significant contributions from the surrounding halides. A distinctive feature was observed for $IrCl_3^-$, where the extra broadness of the X band in the spectrum is attributed to resonant autodetachment, producing spectral features beyond standard Franck–Condon behavior. For $IrCl_5^-$, an orbital rearrangement drives a transformation from a twisted SBP geometry in $IrCl_5^-$ to a more stable TBP structure in singlet $IrCl_5$. This transition is facilitated by reordering of the *d*-orbitals, aligning with the observed shift in spin multiplicity and the calculated VDE. This work provides valuable insights into the reactivity and detachment dynamics of unsaturated iridium halide complexes, potentially informing future studies on ligand exchange reactions and the stability of

This article is protected by copyright. All rights reserved.

14397641, ja, Downloaded from https://chemistry-europe.onlinelibrary.wiley.com/doi/10.1002/cphc.202500170 by Battelle Memorial Institute, Wiley Online Library on [26/05/2025]. See the Terms and Conditions (https://onlinelibrary.wiley.com/terms-and-conditions) on Wiley Online Library for rules of use; OA articles are governed by the applicable Creative Commons License

Accepted Manuscript

dissociative products in transition metal chemistry.

Acknowledgments

The work was partly supported by the National Natural Science Foundation of China (Nos. 92461301, 12250003, and 12034008). X.-B.W. was supported by U.S. Department of Energy (DOE), Office of Science, Office of Basic Energy Sciences, Division of Chemical Science, Geosciences, and Biosciences, Condensed Phase and Interfacial Molecular Science program, FWP 16248.

Conflict of Interests

The authors declare no conflict of interest.

Data Availability Statement

The data that support the findings of this study are available from the corresponding author upon reasonable request.

Keywords: iridium halides · anion photoelectron spectroscopy · density functional theory · d-orbital theory· photodetachment process

References

[1] D. Payne, *Nat. Chem.* **2016**, *8*, 392-392.
[2] F. Chandra, P. Kumar, S. K. Tripathi, S. Patra, A. L. Koner, *Chemmedchem* **2016**, *11*, 1410-1414.
[3] T.-S. Kang, W. Wang, H.-J. Zhong, Z.-Z. Dong, Q. Huang, S. W. F. Mok, C.-H. Leung, V. K. W. Wong, D.-L. Ma, *Cancer Lett.* **2017**, *396*, 76-84.
[4] J.-J. Cao, C.-P. Tan, M.-H. Chen, N. Wu, D.-Y. Yao, X.-G. Liu, L.-N. Ji, Z.-W. Mao, *Chem. Sci* **2017**, *8*, 631-640.
[5] K. Laws, A. Eskandari, C. Lu, K. Suntharalingam, *Chem. Eur. J* **2018**, *24*, 15205-15210.
[6] D.-L. Ma, C. Wu, K.-J. Wu, C.-H. Leung, *Molecules* **2019**, *24*, 2739.
[7] C. Liu, C. Yang, L. Lu, W. Wang, W. Tan, C.-H. Leung, D.-L. Ma, *Chem. Commun.* **2017**, *53*, 2822-2825.
[8] S. J. Thomas, B. Balónová, J. Cinatl, M. N. Wass, C. J. Serpell, B. A. Blight, M. Michaelis, *Chemmedchem* **2019**, *15*, 349-353.
[9] A. J. Carrod, F. Graglia, L. Male, C. Le Duff, P. Simpson, M. Elsherif, Z. Ahmed, H. Butt, G. X. Xu, K. Kam‐Wing Lo, P. Bertoncello, Z. Pikramenou, *Chem.*

This article is protected by copyright. All rights reserved.

Eur. J **2021**, *28*, e202103541.
[10] H. Zhang, L. Zhang, H. Zhong, S. Niu, C. Ding, S. Lv, *Chem. Eng. J.* **2022**, *430*, 132675.
[11] H. A. Zahalka, H. Alper, Y. Sasson, *Organometallics* **2002**, *5*, 2497-2499.
[12] M. V. Jiménez, J. Fernández-Tornos, J. J. Pérez-Torrente, F. J. Modrego, S. Winterle, C. Cunchillos, F. J. Lahoz, L. A. Oro, *Organometallics* **2011**, *30*, 5493-5508.
[13] W. Iali, G. G. R. Green, S. J. Hart, A. C. Whitwood, S. B. Duckett, *Inorg. Chem.* **2016**, *55*, 11639-11643.
[14] D. Matheau-Raven, P. Gabriel, J. A. Leitch, Y. A. Almehmadi, K. Yamazaki, D. J. Dixon, *ACS Catal.* **2020**, *10*, 8880-8897.
[15] M. González-Lainez, M. V. Jiménez, R. Azpiroz, V. Passarelli, F. J. Modrego, J. J. Pérez-Torrente, *Organometallics* **2022**, *41*, 1364-1380.
[16] S. M. King, H. A. Al‐Attar, R. J. Evans, A. Congreve, A. Beeby, A. P. Monkman, *Adv. Funct. Mater.* **2006**, *16*, 1043-1050.
[17] H. Xu, D.-H. Yu, L.-L. Liu, P.-F. Yan, L.-W. Jia, G.-M. Li, Z.-Y. Yue, *J. Phys. Chem. B* **2009**, *114*, 141-150.
[18] J. H. Park, T.-W. Koh, J. Chung, S. H. Park, M. Eo, Y. Do, S. Yoo, M. H. Lee, *Macromolecules* **2013**, *46*, 674-682.
[19] Z. Feng, D. Wang, X. Yang, D. Jin, D. Zhong, B. Liu, G. Zhou, M. Ma, Z. Wu, *Inorg. Chem.* **2018**, *57*, 11027-11043.
[20] E. Pelizzetti, E. Mentasti, C. Baiocchi, *J. Phys. Chem.* **1976**, *80*, 2979-2982.
[21] D. T. Bowron, S. Díaz-Moreno, *Anal. Chem.* **2005**, *77*, 6445-6452.
[22] M. T. Reetz, M. Lopez, W. Grünert, W. Vogel, F. Mahlendorf, *J. Phys. Chem. B* **2003**, *107*, 7414-7419.
[23] R. J. H. Clark, P. C. Turtle, *J. Chem. Soc., Faraday Trans. 2* **1978**, *74*, 2063-2076.
[24] R. J. Deri, J. P. Spoonhower, *Appl. Phys. Lett.* **1983**, *43*, 65-67.
[25] X.-B. Wang, L.-S. Wang, *J. Chem. Phys.* **1999**, *111*, 4497-4509.
[26] J. C. Marcum, J. M. Weber, *J. Chem. Phys.* **2009**, *131*, 194309.
[27] C. Rensing, O. T. Ehrler, J.-P. Yang, A.-N. Unterreiner, M. M. Kappes, *J. Chem. Phys.* **2009**, *130*, 234306.
[28] J. C. Marcum, A. I. Krylov, J. M. Weber, *J. Phys. Chem. A* **2011**, *115*, 13482-13488.
[29] S. M. Matveev, A. S. Mereshchenko, M. S. Panov, A. N. Tarnovsky, *J. Phys. Chem. B* **2015**, *119*, 4857-4864.
[30] S. M. Matveev, D. S. Budkina, I. L. Zheldakov, M. R. Phelan, C. M. Hicks, A. N. Tarnovsky, *J. Chem. Phys.* **2019**, *150*, 054302.
[31] N. Khan, D. Prishchenko, M. H. Upton, V. G. Mazurenko, A. A. Tsirlin, *Phys. Rev. B* **2021**, *103*, 125158.
[32] R. M. Hassan, *J. Mol. Liq.* **2019**, *283*, 302-311.
[33] X. B. Wang, X. P. Xing, L. S. Wang, *J. Phys. Chem. A* **2008**, *112*, 13271-13274.

This article is protected by copyright. All rights reserved.

14397641, ja, Downloaded from https://chemistry-europe.onlinelibrary.wiley.com/doi/10.1002/cphc.202500170 by Battelle Memorial Institute, Wiley Online Library on [26/05/2025]. See the Terms and Conditions (https://onlinelibrary.wiley.com/terms-and-conditions) on Wiley Online Library for rules of use; OA articles are governed by the applicable Creative Commons License

Accepted Manuscript

[34] X. B. Wang, K. Matheis, I. N. Ioffe, A. A. Goryunkov, J. Yang, M. M. Kappes, L. S. Wang, *J. Chem. Phys.* **2008**, *128*, 114307.
[35] M. L. Weichman, J. A. DeVine, M. C. Babin, J. Li, L. Guo, J. Ma, H. Guo, D. M. Neumark, *Nat. Chem.* **2017**, *9*, 950-955.
[36] M. C. Babin, M. DeWitt, J. A. Lau, M. L. Weichman, J. B. Kim, H. Song, H. Guo, D. M. Neumark, *Nat. Chem.* **2023**, *15*, 194-199.
[37] H. Sun, Z. Sun, X.-B. Wang, *Chem. Eur. J* **2024**, *30*, e202402766.
[38] H. T. Liu, C. G. Ning, D. L. Huang, L. S. Wang, *Angew. Chem. Int. Ed.* **2014**, *53*, 2464-2468.
[39] D. L. Huang, H. T. Liu, C. G. Ning, L. S. Wang, *J. Chem. Phys.* **2015**, *142*, 124309.
[40] D. L. Huang, G. Z. Zhu, L. S. Wang, *J. Chem. Phys.* **2015**, *142*, 091103.
[41] L. S. Wang, *J. Chem. Phys.* **2015**, *143*, 040901.
[42] D. J. Goebbert, A. Sanov, *J. Chem. Phys.* **2009**, *131*, 104308.
[43] Q. Zhao, J. Zhang, X. Li, P. Tang, F. Yang, J. Ma, Z. Hu, H. Sun, X.-B. Wang, Z. Sun, Y. Yang, *J. Chem. Phys.* **2024**, *161*, 214305.
[44] P. Tang, J. Zhang, X. Li, F. Yang, Q. Zhao, J. Ma, Z. Hu, H. Sun, X.-B. Wang, Z. Sun, Y. Yang, *J. Phys. Chem. A* **2024**, *128*, 5500-5507.
[45] D. Hanstorp, M. Gustafsson, *J. Phys. B: At., Mol. Opt. Phys.* **1992**, *25*, 1773-1783.
[46] J. Zhang, Z. R. Sun, X. B. Wang, *J. Phys. Chem. A* **2015**, *119*, 6244-6251.
[47] Y. Jean, *Molecular orbitals of transition metal complexes*, Oxford University Press, **2005**.
[48] P. J. Stephens, F. J. Devlin, C. F. Chabalowski, M. J. Frisch, *J. Phys. Chem.* **2002**, *98*, 11623-11627.
[49] S. Grimme, S. Ehrlich, L. Goerigk, *J. Comput. Chem.* **2011**, *32*, 1456-1465.
[50] R. Wesendrup, P. Schwerdtfeger, *Inorg. Chem.* **2001**, *40*, 3351-3354.
[51] G. L. Hou, H. Wen, K. Lopata, W. J. Zheng, K. Kowalski, N. Govind, X. B. Wang, S. S. Xantheas, *Angew. Chem. Int. Ed.* **2012**, *51*, 6356-6360.
[52] J. Joseph, K. Pradhan, P. Jena, H. Wang, X. Zhang, Y. Jae Ko, K. H. Bowen, *J. Chem. Phys.* **2012**, *136*, 194305.
[53] Y. Shi, S. Bian, Y. Ma, Y. Wang, J. Ren, X. Kong, *J. Phys. Chem. A* **2018**, *123*, 187-193.
[54] A. K. Wilson, D. E. Woon, K. A. Peterson, T. H. Dunning, *J. Chem. Phys.* **1999**, *110*, 7667-7676.
[55] D. Figgen, K. A. Peterson, M. Dolg, H. Stoll, *J. Chem. Phys.* **2009**, *130*, 164108.
[56] D. E. Woon, T. H. Dunning, Jr., *J. Chem. Phys.* **1993**, *98*, 1358-1371.
[57] R. A. Kendall, T. H. Dunning, Jr., R. J. Harrison, *J. Chem. Phys.* **1992**, *96*, 6796-6806.
[58] K. A. Peterson, B. C. Shepler, D. Figgen, H. Stoll, *J. Phys. Chem. A* **2006**, *110*, 13877-13883.
[59] K. Raghavachari, G. W. Trucks, J. A. Pople, M. Head-Gordon, *Chem. Phys. Lett.*

This article is protected by copyright. All rights reserved.

14397641, ja, Downloaded from https://chemistry-europe.onlinelibrary.wiley.com/doi/10.1002/cphc.202500170 by Battelle Memorial Institute, Wiley Online Library on [26/05/2025]. See the Terms and Conditions (https://onlinelibrary.wiley.com/terms-and-conditions) on Wiley Online Library for rules of use; OA articles are governed by the applicable Creative Commons License

Accepted Manuscript

2013, *589*, 37-40.
[60] Y. Wei, B.-W. Wang, S.-W. Hu, T.-W. Chu, L.-T. Tang, X.-Q. Liu, Y. Wang, X.-Y. Wang, *J. Phys. Org. Chem.* **2005**, *18*, 625-631.
[61] M. Otsuka, H. Mori, H. Kikuchi, K. Takano, *Comput. Theor. Chem.* **2011**, *973*, 69-75.
[62] J. C. Gómez Martín, O. Gálvez, M. T. Baeza-Romero, T. Ingham, J. M. C. Plane, M. A. Blitz, *Phys. Chem. Chem. Phys.* **2013**, *15*, 15612-15622.
[63] G. W. T. M. J. Frisch, H. B. Schlegel, G. E. Scuseria, M. A. Robb, J. R. Cheeseman, G. Scalmani, V. Barone, G. A. Petersson, H. Nakatsuji, X. Li, M. Caricato, A. V. Marenich, J. Bloino, B. G. Janesko, R. Gomperts, B. Mennucci, H. P. Hratchian, J. V. Ortiz, A. F. Izmaylov, J. L. Sonnenberg, D. Williams-Young, F. Ding, F. Lipparini, F. Egidi, J. Goings, B. Peng, A. Petrone, T. Henderson, D. Ranasinghe, V. G. Zakrzewski, J. Gao, N. Rega, G. Zheng, W. Liang, M. Hada, M. Ehara, K. Toyota, R. Fukuda, J. Hasegawa, M. Ishida, T. Nakajima, Y. Honda, O. Kitao, H. Nakai, T. Vreven, K. Throssell, J. A. Montgomery, Jr., J. E. Peralta, F. Ogliaro, M. J. Bearpark, J. J. Heyd, E. N. Brothers, K. N. Kudin, V. N. Staroverov, T. A. Keith, R. Kobayashi, J. Normand, K. Raghavachari, A. P. Rendell, J. C. Burant, S. S. Iyengar, J. Tomasi, M. Cossi, J. M. Millam, M. Klene, C. Adamo, R. Cammi, J. W. Ochterski, R. L. Martin, K. Morokuma, O. Farkas, J. B. Foresman, and D. J. Fox, Gaussian, Inc., Wallingford CT., **2016**.
[64] T. Lu, F. Chen, *J. Comput. Chem.* **2011**, *33*, 580-592.
[65] W. Humphrey, A. Dalke, K. Schulten, *J. Mol. Graph.* **1996**, *14*, 33-38.
[66] S. Gozem, A. I. Krylov, *Wiley Interdiscip. Rev. Comput. Mol. Sci.* **2022**, *12*, e1546.
[67] M. A. Dobulis, C. J. McGee, T. Sommerfeld, C. C. Jarrold, *J. Phys. Chem. A* **2021**, *125*, 9128-9142.
[68] J. H. Kim, S. H. Lee, J. K. Song, *J. Chem. Phys.* **2009**, *130*, 124321.
[69] Q. Yuan, M. Rohdenburg, W. Cao, E. Aprà, J. Landmann, M. Finze, J. Warneke, X. B. Wang, *J. Phys. Chem. Lett.* **2021**, *12*, 12005-12011.

14397641, ja, Downloaded from https://chemistry-europe.onlinelibrary.wiley.com/doi/10.1002/cphc.202500170 by Battelle Memorial Institute, Wiley Online Library on [26/05/2025]. See the Terms and Conditions (https://onlinelibrary.wiley.com/terms-and-conditions) on Wiley Online Library for rules of use; OA articles are governed by the applicable Creative Commons License

Accepted Manuscript

This article is protected by copyright. All rights reserved.

10.1002/cphc.202500170

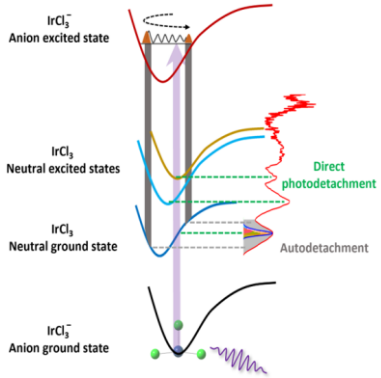

Three undercoordinated iridium chloride anions, $IrCl_n^-$ (n = 3–5), and their neutral counterparts were investigated using cryogenic anion photoelectron spectroscopy and theoretical calculations. The thereotical calculations are in excellent agreement with the experimental results, both revealing superhalogen anion properties characterized by increasing electron detachment energies as chloride ligands are added. When irradiated with the 193 nm laser, the anions $IrCl_4^-$ and $IrCl_5^-$ might undergo photodissociation to produce a Cl^- anion. Subsquently, upon absorbing a second photon, the Cl^- loses an electron, which accounts for the intense characteristics of Cl^- observed in the spectra.The $IrCl_3^-$ anion exhibits a strong absorption feature near 193 nm, inducing a transition to an excited vibrational manifold of the anion. Large-amplitude nuclear motions in these resonant states enable electron detachment that can be projected across a wide range of vibrational levels in the final neutral $IrCl_3$ surface, including highly excited vibrational states not accessible via direct detachment. Consequently, the first band of $IrCl_3^-$ is much broader than the simulation results. After the photodetachment process, the triplet anion $IrCl_5^-$ can transfer to either the singlet state or triplet state. All photodetachment process of the $IrCl_n^-$ (n = 3–5) anions involve the *d*-orbitals of Ir. Following the lose of an electron from $IrCl_n^-$ (n = 3–5) anions, the frontier molecular orbitals of the nutrals are rearranged , accompanied by a change in geometry.

This article is protected by copyright. All rights reserved.

14397641, ja, Downloaded from https://chemistry-europe.onlinelibrary.wiley.com/doi/10.1002/cphc.202500170 by Battelle Memorial Institute, Wiley Online Library on [26/05/2025]. See the Terms and Conditions (https://onlinelibrary.wiley.com/terms-and-conditions) on Wiley Online Library for rules of use; OA articles are governed by the applicable Creative Commons License

Accepted Manuscript